

Structure and Stability of Keplerian MHD Jets

Thibaut Lery^{1,2}, Adam Frank³

¹ Department of Physics, Queen's University, Kingston, ON K7L 3N6, Canada

² Dublin Institute of Advanced Studies, 5 Merrion Square, Dublin 2, Ireland

³ Dept. of Physics and Astronomy, Univ. of Rochester, Rochester, NY 14627-0171

ABSTRACT

MHD jet equilibria that depend on source properties are obtained using a simplified model for stationary, axisymmetric and rotating magnetized outflows (Lery *et al.* 1998, Lery *et al.* 1999a). The present rotation laws are more complex than previously considered and include a Keplerian disc. The ensuing jets have a dense, current-carrying central core surrounded by an outer collar with a return current. The intermediate part of the jet is almost current-free and is magnetically dominated. Most of the momentum is located around the axis in the dense core and this region is likely to dominate the dynamics of the jet. We address the linear stability and the non-linear development of instabilities for our models using both analytical and 2.5-D numerical simulation's. The instabilities seen in the simulations develop with a wavelength and growth time that are well matched by the stability analysis. The modes explored in this work may provide a natural explanation for knots observed in astrophysical jets.

Subject headings: ISM:jets and outflows – MHD – Stars: formation – stability

1. Introduction

Observations of collimated outflows from young stellar objects (YSOs) and active galactic nuclei (AGN) suggest that magnetic fields may play a central role in the physics of these phenomena. Despite the large database of observations, theoretical MHD approaches have not yet converged on answers to several fundamental questions regarding the acceleration, collimation and propagation of these jets (See Lery *et al.* 1999a and reference therein). Difficulties investigating the nature of the jets arise mainly due to the high level of nonlinearity in the governing MHD equations particularly at critical points.

The work presented here is based on a simple model for jet launching and collimation presented in previous articles (Lery *et al.* Lery *et al.* 1998, Lery *et al.* 1999a, hereafter Paper I and II). It yields asymptotic MHD jet equilibria that account for the properties of the emitting source. The model is axisymmetric and stationary and in the work presented here includes more multi-component rotation laws for the source. The model assumes the magnetic surfaces possess a shape which is known a priori inside the fast critical surface, (we refer to the space within the fast surface as the *inner region*) As a first approximation magnetic surfaces were taken to be cones.

The general problem of determining the stationary two-dimensional structure of magnetohydrodynamic outflows requires the solution of the equilibrium of forces perpendicular and parallel to the magnetic surfaces. One can describe the former by using the transfield or Grad-Shafranov equation, and the later using the Bernoulli equation for a polytropic equation of state. Asymptotically, the jet is assumed to be in pressure equilibrium with an external medium whose properties are independent of distance. The transfield and Bernoulli equations are solved both in the inner region and in the *asymptotic region*, which we also will refer to as the *cylindrically collimated regime*.

The stability of the resulting cylindrical equilibria is of major importance, firstly because instabilities could explain observational features of jets such as wiggles, knots or helical filaments, and secondly, because they could be globally disruptive for the outflow. Thus, in this paper, we investigate both the linear stability and the non-linear evolution of our MHD equilibrium jets. This study will provide a diagnostic for features that should develop in fully time-dependent simulations of jet propagation. Such simulations will be the subject of another paper (Frank *et al.* 1999).

Since jet behavior may be directly related to the properties of the emitting source, the models presented here can provide a basis for a better understanding of jet interactions with an ambient medium as well as propagation and stability issues in the context of the nature of the source. The main goals of the present paper are to produce, analyze and study more realistic MHD outflows than simple “top-hat” beams (constant density and velocity) used in previous studies (Frank *et al.* 1998, Cerqueira *et al.* 1999, Gardiner *et al.* 1999, Stone & Hardee 1999). . These new models can then be used as input for numerical simulations. How outflows behave on critical surfaces and in the cylindrical regime constitutes the subject of the first part of the paper. In §2, we briefly recall the main features of the model. Jet equilibria and their properties are presented in §3. Stability analysis and non linear developments of the instabilities for the corresponding equilibria are investigated using ideal MHD computations and numerical simulations respectively in §4. Finally, we summarize the results in §5.

2. The Model

The Given Geometry (GG) model is based on the assumption that magnetic surfaces possess a shape which is known a priori inside the fast critical surface. For full details on the model and on justifications of the approximations, we suggest the reader see Heyvaerts & Norman 1989, and Paper I and II. Inside the fast critical point the three critical points are assumed to be aligned on conical magnetic surfaces. Moreover the angular distribution of magnetic flux is assumed to be uniform. These approximations will be relaxed in forthcoming works.

Unlike the Weber-Davis (1967) type models, however, the balance of forces perpendicular to magnetic surfaces is accounted for on the Alfvén surface and at the base of the flow. On the Alfvén surface the force balance equation becomes what is known as the Alfvén regularity (non-singularity) condition. Owing to axial symmetry, stationarity, as well as the flux freezing condition, there exist in the general case five *integrals of motion* that are preserved on any axisymmetric magnetic surface (denoted a). Two of the integrals, the angular velocity $\Omega(a)$ and a factor related to the entropy $Q(a)$, are given as boundary conditions in the model. These two input functions constitute assumptions about the nature of the source rotator.

MHD flows have two other critical points which are brought about by the Bernoulli equation. There are slow and fast magneto-sonic points both of which are located where the poloidal velocity equals one of the two magneto-sonic mode speeds. The fast and slow surfaces, unlike the Alfvén surface, are saddle points, *i.e.*, transonic solutions only exist for a certain relation among the integrals of motion. These relations are obtained from the criticality conditions that correspond to the vanishing of the differential form of the Bernoulli equation at constant a with respect to ρ and r .

The Alfvén regularity condition together with the criticality conditions determine the three other unknown integrals: namely the specific energy $E(a)$; the specific angular momentum $L(a)$; the mass to magnetic flux ratio $\alpha(a)$. We note that once these integrals are determined the model gives only an approximate solution because the transfield equation is not solved everywhere, but only at a few special places in the *inner region*.

We further assume the density ρ to be related to the pressure p by a polytropic equation of state, $p = Q(a)\rho^\gamma$ where γ is the polytropic index. This assumption replaces consideration of energy balance and is meant to represent simply some more complex heating and cooling processes (See, for example, Vlahakis & Tsinganos 1998 for more general equations of state).

Since the flow eventually becomes fully collimated far from the source, we use

cylindrical coordinates (r, ϕ, z) and assume axisymmetry. R will be the spherical distance centered on the wind source. Each flux surface is labelled by the flux function $a(r, z)$ proportional to the magnetic flux through a circle centered on the axis passing at point r, z . The physical flux is $2\pi a$. We normalize the magnetic flux to the total magnetic flux \mathcal{A} enclosed in the jet, so that a is set to unity on the outer edge. It is convenient to split the magnetic field and the velocity into a poloidal part, which is in the meridional (r, z) plane, and a toroidal part. The former is denoted by a subscript P while the latter is just the azimuthal component. We note that the outflow does not necessarily fill all space from pole to equator.

In the *inner region*, the system is governed by seven equations: the Alfvén regularity condition; the four criticality conditions defined at the slow and fast magneto-sonic points; the Bernoulli equation written at the fast and slow critical points. We note that the number of equations can be reduced to six, due to the conservation of the energy on magnetic field lines. Using these equations the acceleration of the flow is studied up to the fast critical surface. When the flow exits the *inner region*, the flow begins to collimate as field lines bend towards the axis. We do not explicitly follow the collimation process between the fast critical surface (*inner region*) and the *cylindrically collimated region*. We note that between these regions a redistribution of the energy and angular momentum might occur due to shocks or other dissipative process. Nevertheless, the integrals of motion are assumed here to remain exactly the same all along the outflow for simplicity. Therefore, within the framework of the Given Geometry model, the asymptotic flow is uniquely determined from first-integrals obtained from the sub-fast surface regions. In the *cylindrically collimated regime*, the system consists of the asymptotic forms of the Bernoulli and transfield equations. In this region, z goes to ∞ , the flow density ρ is smaller than the Alfvénic density ρ_A , r can be considered to be larger than r_A , and the gravity becomes negligible. The full system of equations remains the same as in papers I and II and is given in Appendix A.

We note again that in the *inner region*, the problem is entirely specified by two functions of a , namely $\Omega(a)$ and $Q(a)$, and also by one constant, the mass-to-magnetic flux ratio on the axis α_0 . In the *asymptotic regime*, only one parameter is needed which can be either the external confining pressure p_{ext} , or the axial density ρ_0 .

Given the properties of the central emitting object, the model allows one to compute the dimensionless rotation parameter $\omega \equiv \Omega r_A / v_{PA}$, where $r_A^2 \equiv L / \Omega$ is the Alfvén radius and v_{PA} the Alfvénic poloidal speed at the Alfvén point $v_{PA} \equiv (\alpha |\nabla \mathbf{a}| / (\rho r))_A$. The density at the Alfvén point is given by $\rho_A \equiv \mu_0 \alpha^2$ and the Alfvénic Mach number by $M_A^2 = v_P^2 / v_{PA}^2 = \rho_A / \rho$. More generally the subscript A will refer to values at the

Alfvén point. Quantities referring to the two other critical points, namely slow and fast magneto-sonic critical points, will be indicated by subscripts s and f respectively. Rotators can be defined as slow, intermediate or fast according to whether the maximum of ω is much less than unity, close to unity, or near its maximum value for of $(\frac{3}{2})^{3/2}$ (See Paper II for details).

2.1. The Rotation Laws

It is now well known that outflows can be accelerated from an accretion disk (“Disk wind”, Blandford & Payne 1982, Pelletier & Pudritz 1992, Fiege & Henriksen 1996, Contopoulos & Lovelace 1994, Ferreira & Pelletier 1993, Ferreira 1997, Vlahakis & Tsinganos 1998, Lery *et al.* Lery *et al.* 1999b), or at the disk-magnetosphere boundary (“X-winds”, Shu *et al.* 1988, 1994). Therefore, a *Keplerian* rotation profile is one of the most realistic description for rotation of sources producing jets. In paper I and II, we have assumed a rigid body rotation. Here, we have chosen more realistic rotation laws by including the *Keplerian* rotation in the outermost part of the outflow. In Fig. 1, the different profiles of angular velocity used in our study are presented. The pure *Keplerian* rotation law (dashed line) starts with a constant rotation close to the axis, as in the rigid body case (dot-dashed lines), but then follows a *Keplerian* profile. The multi-component (solid line), or *multi-fast*, case also starts with a rigid rotation corresponding, for example, to an axial ordinary wind. The angular velocity then doubles its value in order to model a source rotating more rapidly than the star in an intermediate region between the ordinary wind and the Keplerian disc wind that follows. Note that the angular velocity is always sub-*Keplerian* in the intermediate region. For all the rotation laws, the axial value of the angular velocity Ω_0 is set to unity in the figure, and the radius is normalized to the size of the jet. In order to compare fast and slow rotators, we will respectively refer to *multi-fast* and *multi-slow* cases, the latter one rotating four times more slowly.

3. The Jet Equilibrium

3.1. The Numerical Procedure

In the inner part of the flow, the variables calculated in the numerical procedure are the radii r_s , r_f , r_A , and densities ρ_s , ρ_f , ρ_A at the three critical surfaces along with the total energy E . In its cylindrical regime, the jet is entirely defined by r and ρ . All the other physical quantities can be derived from this set. For the numerical calculations, equations

have been reformulated as ordinary differential equations or converted from algebraic conditions into ODEs as functions of the flux surfaces a .

The system consists of eight differential equations, namely the four equations of regularity on slow and fast surfaces (two on each surface), the Alfvén regularity, the conservation of energy (a total of six for the *inner region*), and the Bernoulli and transfield equations in their asymptotic form (for the *cylindrically collimated regime*).

The numerical solutions are obtained by initiating the integration of the system from the axis. Given the input parameters Q_0 , Ω_0 , α_0 , γ , and ρ_0 , all the critical positions and densities can be numerically obtained using analytical formulae (see Paper I). For numerical convenience, we prefer to provide the axial asymptotic density ρ_0 rather than the external pressure. We further constrain the solution to be super-Alfvénic and super-fast-magnetosonic on the axis in the asymptotic region. This gives a limiting range of variations for input parameters and particularly to the axial density ρ_0 .

3.2. The Input Parameters

The input parameters of the model can be selected so as to qualitatively reproduce observations. Given the properties of the jet-emitting object, *i.e.*, its radius R_* , its temperature T_* , the total mass loss rate \dot{M}_* , the base density n_* , the magnetic field B_* , the factor Q_* and γ , it is possible to deduce dimensionless parameters $\bar{\Omega}$, \bar{Q} , $\bar{\alpha}_0$. The parameter $\bar{\alpha}_0$ can be a-posteriori related to the mass loss rate \dot{M}_* , R_* , and the magnetic field B_* . Thus we define $Q_* \equiv 2kT_*n_*/(m_p n_*)^\gamma$, $\alpha_* \equiv \dot{M}_*/4\pi R_*^2 B_*$, and $\Omega_* \equiv \sqrt{GM_*/R_*^3}$. All quantities are non-dimensionalized to reference values by setting $\bar{Q} \equiv Q_*/Q_{ref}$, $\bar{\alpha}_0 \equiv \alpha_*/\alpha_{ref}$ and $\bar{\Omega} \equiv \Omega_*/\Omega_{ref}$. The entropy factor $\bar{Q}(a)$ is assumed to be constant across the jet. We have also studied models where the jet is hotter along the symmetry axis than on its outer edges and find that the results do not significantly change.

In the present paper, we have chosen to model YSO jets with different rotation laws using typical values for T-Tauri stars as presented by Bertout *et al.* (1988) with $M_* = 0.8M_\odot$ and $R_* = 3R_\odot$. At the base of flow, we deduce the corresponding dimensionless input parameters: $\bar{Q} = 0.87$, $\bar{\Omega} = 2$, $\bar{\alpha}_0 = 0.7$, and $\rho_0 = 5 \cdot 10^{-7}$. Major quantities of reference are then given (in CGS) by $R_{ref} = 10^{15} \text{ cm}$, $\rho_{ref} = 250 \text{ ppc}$, $v_{ref} = 10^7 \text{ cm s}^{-1}$ for Young Stellar Objects. The model could be applied to relativistic galactic sources or to quasars, by adapting the reference values and replacing the external pressure of the medium by the inertia of an electro-magnetic field outside the light cylinder in the relativistic regime.

3.3. The Critical Surfaces

The system is solved on the three critical surfaces in the *inner region*. It has been shown in Paper I that the properties of these surfaces are related to the rotation parameter ω . As the parameter increases, the fast and Alfvénic surfaces move apart. In the lower right panel of Fig. 2, the rotation parameter is plotted as a function of magnetic flux. The corresponding input parameters have been given in the previous section. This figure shows that the rotation parameter vanishes at the boundaries and reaches a maximum of 1.6 around $a = 0.45$. Thus the jet generated by this flow will have the properties of a fast magnetic rotator at the location of the maximum in ω . Another relevant quantity $\alpha E/\Omega$ is plotted with the rotation parameter. Its minimum coincides with the maximum in ω . One can show that if this quantity possesses a minimum below its value on the polar axis, the flow will collimate cylindrically (at least for the region inside the minimum). This result is in good agreement with Bogovalov and Tsinganos (1999) who have shown that there always exist field lines that will collimate cylindrically for rotating MHD jets. In our case the cylindrical collimation is ensured due to the pressure of the external medium.

The three critical surfaces and their corresponding densities are represented on Fig. 2, in the upper and lower left panels respectively. The surfaces are distorted with the largest deformation occurring where the rotation parameter reaches a maximum. A relation between the fast and Alfvénic radii has been found in paper I for the fast rotator case that states

$$\frac{r_A}{r_f} \propto \left[\beta \left(3\omega^{\frac{4}{3}} - 2\omega^2 \right)^{\frac{\gamma+1}{2}} \right]^{\frac{3}{2(\gamma-1)}}. \quad (1)$$

This expression shows that when ω approaches its maximum value or when β vanishes, the fast point is pushed far from the Alfvén point. It can even be rejected to infinity in the limiting cases. This is a well known result in the cold plasma limit (Kennel *et al.* (1989)). In our case, β reaches 10^{-2} and $\omega = 1.6$ at the point where the critical surfaces are the most elongated. This behavior has also been obtained in Sakurai (1987) and Belcher & McGregor (1976).

When rotational effects are small ($\omega \approx 0$), *i.e.*, close to the axis, the previous expression becomes $r_A/r_f \propto 1 - 2\omega^2$ (slow rotator case in paper I). Thus the fast point gets closer to the Alfvénic point in these regions.

The slow surface has the opposite behavior compared to the fast and Alfvénic surfaces. It deflates and gets closer to the source as ω increases, as one would expect from $r_s/r_A \propto (r_A/r_f)^{1/3}$ (Paper I). In fact in the fast rotator regime, the slow mode speed gets closer to the sound speed, and the slow mode acquires the character of a sound wave guided along the field line. Thus *the fast magneto-sonic and Alfvén surfaces strongly inflate when*

rotation increases or the flow becoming cold. On the other hand, the slow surface gets smaller with increasing ω .

The lower left part of the figure clearly shows the trend of decreasing densities from the axis to the maximum in ω . At the fast point for fast rotators (see paper I),

$$\frac{\rho_f}{\rho_A} \propto \omega^{-2/3} \left(\frac{r_A}{r_f} \right)^2. \quad (2)$$

The square of the last term explains the decrease of four decades in density. As stated earlier, all the other variables of the problem, such as the first integrals of the motion E , L and α can be deduced from the positions and densities of the critical points. For example, Fig. 2 shows that the total angular momentum reaches a maximum inside the jet and not on the outer edge. Thus *most of the dynamics will be internal* since this quantity is conserved along the flow.

3.4. The Asymptotic Equilibrium

3.4.1. The Numerical Solutions

Here we compare the influence of the rotation laws on the cross-sectional distributions in MHD jets. The quantities that define the jet in the cylindrically collimated regime are plotted in Fig. 3 for pure *Keplerian*, *multi-fast* and constant rotations. The z and ϕ components of velocity and magnetic field are represented together with the density ρ and the net electric current I_C , as functions of the relative radius (normalized to the jet radius). The length scale is the jet radius. The density is normalized to its value on the jet axis ρ_0 . The non-dimensional velocities refer to the fast magnetosonic velocity $v_f^2 = c_s^2 + v_A^2$ on the axis, c_s being the sound speed. The magnetic field is normalized to $\sqrt{\rho_0} v_f$.

The poloidal velocity v_z increases from the axis to the outer edge for the rigid rotation case, and slightly decreases for the pure *Keplerian* case. For the *multi-fast* case, however, v_z peaks where the rotation parameter is maximum, approximately in the middle of the jet. Therefore in the latter case, the fastest part of the jet is neither on the axis or on the outer edge, but inside the jet itself. The azimuthal velocity v_ϕ follows the same trend but with a magnitude several orders smaller than the poloidal component. If v_z is of the order of several hundreds of $km s^{-1}$, v_ϕ is only about a few $km s^{-1}$.

The azimuthal component of the magnetic field always dominates the poloidal part except at the axis. Thus for these parameters the jet's field is highly twisted. The azimuthal component B_ϕ follows approximately a $1/r$ law in the outer part.

As one moves towards the axis from the edge of the jet magnetic pinch forces or *hoop stress* become increasingly important. In order to maintain an equilibrium the gas pressure must balance the hoop stresses. Thus we see large pressure and density gradients in near the axis. We denote the high density region centered on the axis as the *core*, and the lower density outer regions as the *collar*. Note that the bulk of the jet’s momentum resides in the core. Hence this portion of the beam will penetrate more easily into the ambient medium during the jet’s propagation while the collar will be more strongly decelerated. Thus we expect that even if the relative velocity is smaller close to the axis, the central part of the flow will propagate faster.

The last quantity represented in Fig. 3 is the ”poloidal electric current” through a circle centered on the axis and extending out to a magnetic surface a . This quantity is given by $I_C(a) = -rB_\phi/\mu_0$ (The physical poloidal current is $I_{phys} = -2\pi I_C$). While the current is always increasing for a constant rotation jet, in the *Keplerian* and multi-component models it reaches a maximum in the middle of the beam and vanishes at the outer boundary. Therefore a return current flows back inside the jet in these cases. This will be studied in more detail for the *multi-fast* case in the next section.

The kinetic to Poynting flux ratio (not shown here) can be calculated as a function of the relative radius. We find that only the central part of the asymptotic outflow has a kinetic energy flux strongly dominating the Poynting flux. Thus away from the axis a non-negligible part of the magnetic energy is not transformed into kinetic energy.

Thus *rigid body rotation jets are characterized by a dense, current-carrying core having most of the momentum, surrounded by a tenuous current-free envelope, dominated by the azimuthal magnetic field. Keplerian and multi-fast cases also exhibit a central current-carrying core but are surrounded by a denser collar and carry an internal return current.*

3.4.2. An Approximate Analytical Solution

By simplifying the asymptotic equations, it is possible to obtain approximate analytical solutions in the region where the jet is cylindrical. Away from the axis, where the gas pressure is negligible with respect to magnetic pressure, the transfield equation can be integrated to yield $\Omega^2 r^4 \rho^2 \mu_0^{-1} \alpha^{-2} = \text{constant}$. Then the density can be expressed as a function of r and of the first integrals

$$\rho(r) \approx C\alpha/\Omega r^2, \tag{3}$$

where C is a constant. In the present work, the angular velocity $\Omega(r)$ is given as an initial condition, while the mass to magnetic flux ratio $\alpha(r)$ is part of the solution. If $\alpha(r)$ and $\Omega(r)$ are constant, the density drops as r^{-2} . This is the behavior that we get for the rigid body rotator away from the axis. On the other hand, for increasing α , or decreasing values of Ω , the density can increase as obtained for the *multi-fast* rotator in the outer regions of the jet. Close to the axis, *i.e.*, $r \ll 1$, the gas pressure dominates and the density approaches a constant, the transfield equation reducing approximately to $Q\rho^\gamma = \text{constant}$.

The above result allows one to derive similar approximate formulae for the toroidal components of the magnetic field and velocity which respectively reduce to $|B_\phi| \approx \Omega\rho r/\alpha$, and $|v_\phi| \approx \rho\Omega r/\mu_0\alpha^2$. Combined with Eq. 3, the equations become

$$|B_\phi(r)| \approx C/r \quad , \quad |v_\phi(r)| \approx C/\alpha. \quad (4)$$

It follows that the net asymptotic electric current is approximately given by $I = 2\pi r|B_\phi|/\mu_0 \approx \text{constant}$. Therefore, in the region where magnetic pressure dominates over gas pressure, the asymptotic current will be constant. Finally, one can deduce the asymptotic poloidal velocity of the flow $v_z(r) = (\alpha/\rho r)da/dr$, that becomes

$$v_z(r) \approx \Omega r/C. \quad (5)$$

Fig. 4 shows the approximate analytical solutions together with the solution for the *multi-fast* case. The density and the poloidal velocity are well reproduced in the intermediate region where the magnetic pressure dominates. The toroidal component of the magnetic field is well described by the formula only far from the axis. Finally, the toroidal component of the velocity is similar in the analytical and the numerical solutions.

In theory, by using this approximate solution, it may be possible to deduce the properties of an outflow and, therefore, of the emitting object directly from quantities observed in the jets. A rough estimate of α could be deduced from the toroidal component of the velocity. Combined with an accurate measure of the density and of the asymptotic axial velocity, it would give the angular velocity. Using the model, the five first integrals could be estimated and would allow a characterization of the source itself. Moreover, just from the profile of the density, it would be possible to deduce the mass to magnetic flux ratio, $\alpha(r)$, for a given rotation law. Thus *a precise measure of the mass density in jets may be a key point in order to deduce the properties of the source at its base.*

3.5. The Current along the Jet

In Fig. 5, we present the net electric current on the Alfvénic and fast surfaces and in the *cylindrically collimated region*, in order to have a global picture of the current circulation in the jet. Only the *multi-fast* case is presented here since the *Keplerian* case presents similar trends. The current first increases outwards from the axis, then reaches a plateau where the magnetic pressure dominates, as shown in the previous section. Finally, it decreases in the outer part of the jet, and almost vanishes on the outer boundary. The current density is negative in the outer part of the jet and therefore the direction of the current is opposite to the one in the axial region. Thus *there exists a strong current in the core and a return current in the collar, the intermediate part of the jet being almost current-free.*

We note that the current is never strictly zero on the outer boundary, and therefore a small part of the current may flow back either on the external surface of the jet, or in the external surrounding medium. This result is similar to the force-free field model of Lynden-Bell (1996), where the current circulates inside the jet itself, and where the magnetic field lines are anchored in a differentially rotating accretion disc.

3.6. Comparisons with Previous Works

The characteristics of magnetized outflows at large distances from the central object have been addressed by a variety of studies. Many results of the present study are in good agreement with these works. For example, as found by Beskin *et al.* (1998), a jet with a zero total electric current has its angular velocity vanishing at the jet boundary, and its axial regions dominated by kinetic energy. Concerning the current, Bogovalov (1995) has shown analytically that there always exists a field line in the outflow which encloses a finite total current, and consequently, the asymptotics always contain a cylindrically collimated core. This is precisely what we find in the axial region of our jets, regardless of the presence of any external medium that would ensure cylindrical collimation anyway. As with Ferreira (1997), it is possible to show, as it is done in paper I, that the minimum mass loss rate has a lower limit and can not be arbitrarily small. We also agree with Ostriker (Ostriker 1997) and Lery *et al.* (Lery *et al.* 1999b) who conclude that the optical jet may represent only the densest part of the total outflow.

We obtain fast magnetosonic Mach numbers, (which also corresponds to the Alfvénic Mach number on the axis), between 2 and 4. This range corresponds to what Camenzind (1997) has found for his model for low-mass protostellar objects. The corresponding jets have low fast magnetosonic Mach-numbers $M_A \simeq 2$. By taking into account an

accretion disc around the stellar magnetosphere, Fendt & Camenzind (1996) also find a fast magnetosonic Mach-number ≈ 2.5 . However, this does not seem to be a general statement about MHD jets since there exist models with larger values (Sauty *et al.* (1994), Trussoni *et al.* (1997)).

Shu *et al.* (1995) have studied magneto-centrifugally driven flows from young stars including their structure at large distances from the source when they collimate into jets. When $R \gg 1$ and r is at least moderately large also, they have found that the density distribution can be given by $\rho \rightarrow K(r)/\alpha(r)r^2$ (their Eq.4a) where $K(r)$ is an arbitrary (but slowly varying) positive function of r . This result, and the variations of their asymptotic velocity, are in good agreement with Eq. 3, with $K(r)$ being $C/\Omega(r)$ in the present model. Despite the similarity of the analytical results, the functions in Shu *et al.* do not correspond to the *multi-fast* (nor the *Keplerian*) case. Note that our model does not describe the physical processes occurring at the source itself, *i.e.*, at the surface of the disk or the disk-star boundary. Thus one may be able to link our results to models such as Shu’s for the generation of the outflow at its source.

3.7. The Astrophysical Consequences

The model makes it possible to obtain MHD jet equilibria with multiple components, *i.e.*, a central dense core surrounded by a collar. Characteristic physical quantities are close to those obtained observationally, with, for example, velocities of several 10^2 km s^{-1} for YSOs. We note that there exists a broad range of solutions to the equations that possess favorable characteristics for comparisons with observations. Moreover, the properties of the different parts of the jet can be directly related to the properties of the source. Therefore the ensuing equilibria can be used to simulate numerically the propagation of the jet into an external medium, more realistically than with a “top-hat” distributions for velocity and density. By comparing astrophysical observations with the results of different simulations of jet propagation could ultimately provide a tool for deriving source properties.

Another important issue that must be addressed is the effect of ambipolar diffusion in our model, and the estimation of the distance where it should become effective. In a recent work by Frank *et al.* (1999), it has been shown that the ambipolar diffusion time-scale was related to the plasma β parameter, $\beta \equiv P_g/P_B$, by

$$t_{ad} = 28,904 \left(\frac{n_n}{10^3 \text{ cm}^{-3}} \right) \left(\frac{r_{jet}}{10^{15} \text{ cm}} \right)^2 \left(\frac{10^4 \text{ K}}{T_{jet}} \right) \left(\frac{\beta}{\beta + 1} \right) \text{ y}. \quad (6)$$

In this equation, the ambipolar diffusion time-scale is given in years, n_n is the number density of neutral particles, and T_{jet} is the temperature. When $\beta \rightarrow \infty$, the term $\beta/(\beta + 1)$

tends to unity, while when $\beta \ll 1$, the ambipolar diffusion time-scale can be effectively reduced. In the present model, the plasma β parameter is given by

$$\beta(a) = \frac{2\gamma}{(\gamma - 1)} \frac{Q\rho_A^{\gamma-1}}{v_{PA}^2}. \quad (7)$$

As shown in Fig. 6, β can become quite low in some part of the jet. The most dramatic case is the *multi-fast* case, where value around 10^{-2} can be reached in the intermediate part of the jet, the core and the collar having a plasma parameter larger than unity. Therefore, the jet is magnetically dominated only in the intermediate zone, precisely where ambipolar diffusion can be effective. For all the other cases, the average value of the parameter is about unity. From observations, typical values for YSO jets are: $10^3 \leq n_n / \text{cm}^{-3} \leq 10^4$; $1 \times 10^{15} \leq r_{jet} / \text{cm} \leq 5 \times 10^{15}$; $5 \times 10^3 \text{ K} < T < 3 \times 10^4 \text{ K}$ (Bacciotti & Eisloffel 1999). For jet parameters in the middle of the expected range of variation, we find t_{ad} of order 10^5 to 10^4 y. Thus the dynamical time-scale for YSO jets is $t_{dyn} = 10^4 - 10^5$ y (Reipurth *et al.* 1997, Eisloffel & Mundt 1997). This is of order of, or greater than, the ambipolar diffusion time: $t_{dyn} > t_{ad}$. If we consider length scales, the distance D_{ad} , where ambipolar diffusion becomes effective is approximatively between 0.1 pc and 3 pc , for jet velocities around 10^2 km s^{-1} . This is the range of distances where the magnetic field might be altered or at least where internal configurations should evolve. Such an effect should reduce the internal *hoop stress* that would normally help the jet to remain collimated. It could also reduce instabilities as it will be shown in the next section. Hence, parsec scales YSO jets should naturally be less collimated when $t_{dyn} \approx 10^4 - 10^5$ y.

Finally, the present jet equilibria show large gradients in velocity, magnetic field and density. Such configurations should give rise to instabilities that could change internal structures of jets or even disrupt them. This is the subject of the next section.

4. The Stability Analysis

Current-carrying jets with a helical fields are susceptible to pressure-driven (PD), Kelvin-Helmholtz (KH) and magnetic instabilities driven by the electrical current (Current Driven, CD). The latter modes are due to field aligned electrical currents. Generally instabilities will be a mixture of CD, PD and KH modes with the contributions from each type of mode being difficult to estimate. Stability properties of such MHD jets have been investigated only recently (Appl & Camenzind 1993, Appl 1996, Lery Lery 1996, Appl *et al.* 1999). These instabilities could play an important role in various observed morphological structures such as wiggles, (*e.g.* for quasars: Krichbaum *et al.* 1990, Feretti *et al.* 1999, for YSO jets: Schwartz & Greene 1999), knots (*e.g.* for YSO jets: Ray *et al.* 1996, Raga

& Noriega-Crespo 1998, Rosado *et al.* 1999), and filaments (*e.g.* for AGNs: Biretta 1996, Bahcall *et al.* 1995, for YSO jets: Elmegreen 1989, Dutrey *et al.* 1991).

4.1. The Linear Stability Analysis

In order to study linear development of instabilities, we adopt the standard (temporal) approach where the axial wavenumber k is real and the imaginary part of the complex frequency corresponds to growth rate Γ , growth time being $\tau = \Gamma^{-1}$. Wavenumbers are given in units of inverse jet radius and growth rate is normalized to the inverse Alfvén time. A synopsis of the method is presented in Appendix B.

4.1.1. The Pinch Mode $m = 0$

Stability analysis of magnetic configurations derived from the Given Geometry model have been studied in Lery (Lery 1996) for rigid rotators. We report here the main results. It has been shown, in such a case, that the pinch, or sausage, mode ($m = 0$) dominates over other m -th order modes. This is mainly due to the large gradients of the density and of the magnetic field that create strong PD and CD instabilities respectively.

The results of (Lery 1996) show that pure CD modes can develop on rapid, *i.e.*, Alfvén, time scales. Moreover fast rigid rotators are more unstable than slow ones. In Fig. 7, we have plotted the dispersion relation for these two cases for the pinch mode $m = 0$. By studying a large range of angular velocities, Lery (Lery 1996) demonstrated that faster rotation rates produce larger growth rates and smaller wavenumber cut-offs. This is clearly seen in the figure, where the fast rotator is the most unstable for large wavelengths (*i.e.*, small wavenumbers), but also presents a smaller cut-off in wavenumbers. The maximum growth rates and their corresponding wavenumbers are reported in table 1. The unstable modes that should grow the most rapidly have a wavelength about 3 jet radii for the fast rotators and half the jet radius for the slow rotators. These results can be applied to observations of real YSO jets. For HH34 the largest wavelength above corresponds approximately to the minimum knot separation of $3.4 r_{jet}$ as given by Burke *et al.* (1988). In the case of HH111 however, the separation is larger, about $11 r_{jet}$ (Reipurth 1989, Morse *et al.* 1998). Thus model seems not to fit to the HH111 case. If the jet diameter is not defined as the full width of the jet, $2 r_{jet}$ as we have done, but as the observationally deduced knot width then the application appears better. This would correspond, in our model, to the denser, axial core. In such a case, the jet diameter would be smaller by a

factor of 3 or 4 and knot separation would be about 9 to 12 r_{jet} , thus accounting for the larger separation of knots of HH111.

We note also that the number of knots for HH111 is about 13 (Reipurth 1989) corresponding to an approximate length of the knotted section of the jet of $4 \times 10^{17} \text{ cm} = 0.13 \text{ pc}$, (given a knot separation of $3 r_{jet} = 3 \times 10^{16} \text{ cm}$. This is the distance where *ambipolar diffusion* could become effective in the jet, as pointed out earlier in the present paper. Therefore, at 0.1 pc from the source, the internal configurations should begin to evolve leading to decreases in pressure and magnetic field gradients. Consequently pressure driven and current driven instabilities should be less important. This might be the reason for the disappearance of the knots at this distance from the source.

Thus, *regardless the type of rotators, the domination of axisymmetric modes and their corresponding wavelengths suggest that these instabilities could be at the origin of the knotted structures seen in a large number of jets as seen, for example, in HL Tau, HH1, HH30 and HH34 (Ray et al. 1996), or in HH11 and HH311 (Rosado et al. 1999).*

This potential origin for knots has already been proposed by several authors (Burke *et al.* 1988, Bodo *et al.* 1995, Micono *et al.* 1998). These studies focused on Kelvin-Helmholtz instabilities. Todo *et al.* (1992), however, have argued that the pure KH instabilities could not alone produce the knots. We propose that *the knots may be due to the combined effects of the KH, CD, and PD instabilities, with a domination of the PD and MHD instabilities.*

4.1.2. The Helical Mode $|m| = 1$

As stated above an MHD outflow can exhibit Kelvin-Helmholtz, current-driven, and pressure-driven instabilities. In general, it is not possible to entirely separate these modes. Only with very simple and idealized configurations one can hope to understand the physics driving individual modes. In this section we restrict ourselves to current-driven modes, in order to study their effects on our models. We use the results obtained by Appl *et al.* (1999). They have approximated the MHD jet by an infinitely long cylindrical outflow of a perfectly conducting plasma. The jet is supposed to have constant density and velocity, as well as negligible thermal pressure and rotation. Consequently, Kelvin-Helmholtz instabilities arise only due to the vortex sheet at the jet boundary. Moreover, pressure-driven instabilities are excluded by considering cold jets. The simplifications differ from our present model, *i.e.*, we have velocity and pressure gradients. Nevertheless it allows to get a *rough estimate* of the maximum growth rate and wavenumber for each value of the axial pitch. Eventually the ensuing characteristic wavelengths can be calculated.

Appl *et al.* (1999) have shown that CD helical modes generally dominate in their jet configurations. They found that the magnetic pitch, $P = rB_z/(r_{jet}B_\phi)$, and in particular its value on the axis, P_0 , essentially determines the growth rate of the helical instabilities in the case of small values of the pitch. We have plotted the pitch in Fig. 8 (left panel) as a function of the relative radius, for *Keplerian*, *multi-slow* and *multi-fast* rotators. The axial values of the pitch functions were deduced from the models presented above. Following the same procedure as Appl *et al.* (1999), it is possible to derive the maximum growth rates and wavenumbers as functions of the axial pitch for our jets (right panel in Fig. 8). Results are reported in table 2. The most unstable magnetic configurations correspond to the *multi-slow* case which has a very small wavelength. We note that the *Keplerian* and *multi-fast* cases have maximum growth rates that are still quite large.

One should note that the maximum growth rates given here have been obtained for a particular value of medium external pressure. An increase of the external pressure increases the central pitch P_0 which reduces Γ_{max} by a factor of 10. For large external pressure, the pinch mode can be of the same order or larger than the helical mode. A 3D simulation would be needed in order to study the development and the evolution of these instabilities in detail.

4.2. The Non-linear Evolution

4.2.1. The Kink Modes

Non-linear computations of the development of the CD modes have been carried out by Lery, Baty & Appl (Lery *et al.* 1999c) using a cylindrical evolution code. These calculations show that like the linear evolution, non-linear instabilities also develop on rapid time scales and therefore should affect internal jet structures. Moreover the non-linear behavior of the jet equilibrium is highly sensitive to the structure of the initial magnetic configuration. In the present case where the pitch function is increasing, the dominant mode ($m = 1$) is most probably resonant at half the relative radius of the jet. A current sheet should form at this locus producing a kinked inner cylinder due to helical distortion. Reconnection and turbulence in such a configuration should occur and accelerate particles on this surface. The ensuing saturated configurations may look like a hollow cylinder. For AGNs, such a structure may be related to the formation of the VLBI knots, which apparently are non-axisymmetric features within the flow channel (Krichbaum *et al.* 1990). Finally, a high current density forms along the jet axis in these calculations. This should give rise to radially localized dissipation which could be a potential heating mechanism within the jet core.

4.2.2. The Simulations

The Numerical Method A multi-dimensional (2.5-D) simulation of a *multi-fast* MHD jet have been performed using a MHD TVD code in cylindrical symmetry (see Ryu, Jones & Frank 1995a and Ryu *et al.* 1995b). The simulations are initiated with the cylindrically collimated jet equilibrium traversing the length of the computational domain (256×1024 zones), the jet radius being 64 zones. The equilibrium is then continuously injected at $z = 0$ boundary of the grid. The radius of the jet was chosen to correspond to a YSO jet of 10^{16} cm. The maximum density of the initial jet was 250 *ppc*, and the central velocity was 10^7 cm s^{-1} . The pressure outside the jet was imposed by the model through the pressure balance at the outer boundary. The jet is surrounded, in the present simulation, by a magnetized medium that has a small poloidal field and no toroidal component.

As seen previously, the present magnetic configuration is always unstable to both the pinch and the helical (or kink) modes. Since our simulation is axisymmetric, it is only possible to track the pinch modes. In order to study the kink modes 3D simulations are required. This will be the subject of a forthcoming paper.

The Results We note first that the equilibrium remains stable over a long period. No preferential perturbation has been used in order to destabilize the simulation. As the jet propagates numerical noise generates the instabilities. Two types of regularly spaced features arise. One has a small wavelength and is located close to the axis. The second presents a larger wavelength. the second mode is wider and situated at the interface between the jet and the ambient medium as illustrated in fig. 9 and fig. 10 where the density, and the poloidal and toroidal components of the magnetic field are shown respectively.

In a companion paper (Frank *et al* 1999) we have performed simulations which follow the propagation of the jet models presented here. These simulations also show instabilities developing in the beam which have identical wavelengths. The instabilities are initiated where the beam interacts strongly with ambient medium via the propagation. Here the instabilities take longer to develop as they are generated via low level noise. Note the form of the instability at the axis. Detailed inspection of the simulations show a strong axial flow (a pinch). When material reflects off the axis it expands in a tight balloon or loop-like structure. As the flow evolves each loop interacts with its neighbor leading to a saturation of the growth. Consideration of the poloidal and toroidal fields shows that initially the loops are dominated by the toroidal components.

In Fig. 9, the gray-scale map of the density, we have drawn schematically the envelope of the largest instabilities (dashed line) and marked by large arrows the corresponding

location of the knots. The smallest internal instabilities are also shown by smaller grey arrows. We note that there exist globally five small instabilities between two consecutive knots of the envelope. The corresponding wavelengths are reported in table 3. The corresponding wavenumbers are also provided.

We note that the wavelength of the envelope is around $3r_{jet}$ and that the smallest instabilities correspond to half the jet radius. As shown by Appl *et al.* (1999), current driven instabilities are absolute instabilities, *i.e.*, they grow but do not propagate, in the rest frame of the jet, and the boundary conditions at the outer edge of the jet do not affect the internal modes. Hence internal instabilities will develop first as seen in Fig. 9. On the other hand, the instabilities with large wavelengths that develop on the envelope will directly depend on the the boundary of the jet that is only perturbed when the internal instabilities become important. Thus *in real astrophysical jets, small internal instabilities should develop before larger ones which give rise to the larger pinches of the jet.*

4.3. Comparison of the Results

Since our simulation is axisymmetric and therefore only track the pinch modes, the results of the simulation can only be compared with those presented in section 4.1.1.

In the axial part of the jet, the rotation parameter ω is small with respect to unity. Following the classification of paper I, this corresponds to the characteristic of a slow rotator. Hence, for our simulation, the instabilities in the core should be related to the results presented in table 1 for the slow rotator. On the other hand, in the intermediate and the outermost regions, the jet properties correspond to those of a fast rotator. The largest growth rate for the fast rotator corresponds to that of the envelope. These wavelengths have been reported in table 4, together with their ratio, and show good agreement.

The first internal instabilities arise at around $5 r_{jet}$ in the simulation. They grow and become important at about $10 r_{jet}$. The mean time for the instabilities to grow is then approximatively given by

$$\tau_I \approx 5 r_{jet}/v_{jet}. \quad (8)$$

Let us compare this with the growth time of the pinch mode instabilities τ_{slow} for the slow rigid rotator. The inverse of the maximum growth rate for slow rotator (table 1) gives it as $\tau_{slow} = \Gamma_{slow}^{-1} = 1.5 \tau_A$, where $\tau_A = r_{jet}/v_A$ is the Alfvén time. Using the value of the relative velocity in Fig. 3 (upper left panel), we can derive the velocity of the jet w.r.t. the Alfvén velocity, *i.e.*, $v = v_{jet}/v_A \approx 3 \pm 0.5$. Then the Alfvén time is approximately given by

$\tau_A \approx 3(\pm 0.5)r_{jet}/v_{jet}$. Hence we finally have

$$\tau_{slow} = 1.5 \tau_A \approx 4.5 (\pm 0.75) r_{jet}/v_{jet}, \quad (9)$$

that can be compared to τ_I . Hence the instabilities develop in the simulation as predicted by the stability analysis. Moreover these growth times are rather short and consequently the internal instabilities in astrophysical jets should develop relatively close to the source (at about $5 r_{jet}$).¹

Thus the theoretical results are in good agreement with the simulations. The present stability analysis seems to be a good diagnostic tool to understand the development of instabilities in MHD jets, and to predict their characteristic wavelengths.

5. Conclusions

In this work we have investigated Keplerian MHD jet equilibria by means of a simplified axisymmetric, polytropic and stationary model. It assumes that the magnetic surfaces possess a shape, conical in the present case, which is known a priori inside the fast critical surface. In this *inner region*, the problem is entirely specified by $\Omega(a)$, $Q(a)$, and α_0 . The Alfvén regularity condition together with the criticality conditions determine the three other unknown first integrals: $E(a)$, $L(a)$ and $\alpha(a)$. In the *asymptotic region*, the flow is uniquely determined by the first-integrals obtained in the *inner region* together with the axial density ρ_0 which is given as boundary condition. This region is governed by the asymptotic forms of the Bernoulli and transfield equations. Our principal conclusions can be summarized as follows:

1. In the *inner region*, we find that the fast magneto-sonic and Alfvén surfaces strongly inflate when rotation increases, while the slow surface gets smaller. The fast point remains at a finite distance for finite entropy flows, in contrast to cold flows.
2. In the *asymptotic region*, jets have a dense and current-carrying central core where most of the momentum is located. Rigid body rotation jets are surrounded by a tenuous current-free envelope, dominated by the azimuthal magnetic field. *Keplerian* and *multi-fast* jets are surrounded by a denser collar and carry an internal return current. The intermediate part of the jet is almost current-free and is magnetically dominated.

¹ As shown by Begelman (1998), the distance R_{min} from the source where instabilities start growing in a non-relativistic, supersonic jet must be larger than $M_A r_{jet}$ (in our case $R_{min} > 2.5 r_{jet}$).

3. An approximate analytical solution was derived which may make it possible to estimate the properties of the outflow and of the emitting object directly from the quantities observed in jets, *e.g.* the density, the components of the jet velocity.
4. We have addressed the linear stability and the non-linear development of instabilities for the corresponding equilibria using both analytical and 2.5-D numerical simulations. Instabilities in the simulations develop with a wavelength and growth time that are well matched by the stability analysis. Regardless the type of rotators, the wavelengths of the axisymmetric modes suggest that these instabilities could be at the origin of the knotted morphology of a large number of astrophysical jets.
5. The rather short growth times of the internal instabilities suggest that they should develop relatively close to the source, at about $5 r_{jet}$ for YSO jets.
6. We have shown that ambipolar diffusion should be effective on times scales of order 10^4 to 10^5 y, or a length scale equal or larger than $0.1 pc$, at least in some part of typical YSO jets. The consequent changes of the internal magnetic configurations might be the reason for the disappearance of knots at such a distance from the source, as observed.
7. The relatively good agreement between the theoretical results and the simulation shows that the present stability analysis is a good diagnostic tool to understand the development of instabilities in MHD jets.

We wish to thank Hubert Baty, Stefan Appl, Jean Heyvaerts for their help with this project. We thank Tom Gardiner and Guy Delamarter for useful discussions and Tom Jones and Dongsu Ryu for their help with the numerical code. This work was supported by NSF Grant AST-0978765 and by the University of Rochester’s Laboratory for Laser Energetics. The project was also supported by an operating grant from NSERC of Canada.

A. The Differential Equations of the Model

1. The so-called *Alfvén regularity condition* is the particular form assumed by the force balance perpendicular to the magnetic field, or transfield equation, at the Alfvén point. It can be written as

$$\frac{\alpha'}{\alpha} + 2(1-p)\frac{r'_A}{r_A} - 2(1-p)\frac{\sin\theta_A}{r_A|\nabla a|_A} - \frac{Q\rho_A^{\gamma-1}}{(\gamma-1)v_{PA}^2} \frac{Q'}{Q}$$

$$+\frac{E'}{v_{PA}^2} + \frac{\Omega^2 r_A^2}{v_{PA}^2} \left(\frac{\alpha'}{\alpha} \frac{1}{(1-p)^2} + 2 \frac{r'_A}{r_A} \frac{p}{1-p} - \frac{\Omega'}{\Omega} \right) = 0, \quad (\text{A1})$$

where p is the slope of the solution of the Bernoulli equation at the Alfvén point. The reader should see Heyvaerts & Norman 1989, Lery *et al.* 1998 and Lery *et al.* 1999a for a more detailed explanation of the equations and methods

2. The projection of the equation of motion on \mathbf{B}_P yields by integration the *Bernoulli equation*, $E(a) = v^2/2 + (\gamma/(\gamma-1))Q\rho^{\gamma-1} + G(r, z) - r\Omega B_\theta/\mu_0\alpha$. In the absence of MHD forces, this first integral would express the well known Bernoulli's theorem, i.e. the constancy of the sum of the kinetic, enthalpy and gravitational energy fluxes. The presence of the magnetic field introduces another energy flux, the Poynting flux, the fourth term in the equation. The total specific energy has a given value on a magnetic surface. This can be expressed in differential form as

$$\frac{d}{da}(E_s - E_f) = 0. \quad (\text{A2})$$

where the s and f subscripts refer to the slow and fast points respectively

3. Every solution has to fulfill *four criticality conditions* defined at the slow and fast magneto-sonic points. These points are located where the differential with respect to ρ and r of the Bernoulli function $\mathcal{B}(r, \rho) = E(a)$ vanishes, i.e., $r\partial\mathcal{B}/\partial r = 0$, $\rho\partial\mathcal{B}/\partial\rho = 0$. It is convenient to convert the algebraic magnetosonic criticality conditions into differential equations. The critical points can be followed from one magnetic surface to the next by differentiating these criticality equations with respect to a :

$$\frac{d}{da} \left(\frac{\partial\mathcal{B}}{\partial r} \right)_s = 0 \quad , \quad \frac{d}{da} \left(\frac{\partial\mathcal{B}}{\partial\rho} \right)_s = 0 \quad (\text{A3})$$

$$\frac{d}{da} \left(\frac{\partial\mathcal{B}}{\partial r} \right)_f = 0 \quad , \quad \frac{d}{da} \left(\frac{\partial\mathcal{B}}{\partial\rho} \right)_f = 0. \quad (\text{A4})$$

4. The *asymptotic form of the Bernoulli equation* can be written as:

$$\frac{dr}{da} = \alpha \left[\rho r \sqrt{2} \sqrt{E - \frac{\gamma}{\gamma-1} Q \rho^{\gamma-1} - \frac{\Omega^2 r^2 \rho}{\mu_0 \alpha^2}} \right]^{-1}. \quad (\text{A5})$$

5. The asymptotic form of the transfield equation is given by:

$$r^2 \frac{d}{da} (Q\rho^\gamma) + \frac{1}{2} \frac{d}{da} \left(\frac{\Omega^2 r^4 \rho^2}{\mu_0 \alpha^2} \right) = 0. \quad (\text{A6})$$

B. The Stability Analysis Method

A global normal mode stability analysis is used. The radial displacements, ξ_r , of the fluid elements from their equilibrium positions are of the form,

$$\xi_r(\vec{x}) = \xi_r(r) \exp i(m\phi + kz - \omega t) \quad (\text{B1})$$

and similarly for the remaining perturbed quantities. The linearized equations can be cast into a system of two first order ODE for $Y \equiv r\xi_r$ and the total perturbed pressure $Z \equiv \delta p_{\text{tot}} = \delta(p + B^2/8\pi)$. It is given by

$$AS \frac{dY}{dr} = C_1 Y - rC_2 Z, \quad (\text{B2})$$

and

$$AS \frac{dZ}{dr} = C_3 Y/r - C_1 Z, \quad (\text{B3})$$

where A, S and C_i functions of the equilibrium quantities as well as the Fourier parameters ω, k, m (Appl & Camenzind 1993).

Jets propagate through a compressible medium of high conductivity. Since one is interested only in instabilities due to the jet itself, radially outgoing decaying waves for large radii define the boundary condition,

$$P \propto H_m^{(1)}(\lambda r) \quad (\text{B4})$$

for $r \rightarrow \infty$. The $H_m^{(1)}$ are the Hankel functions of the first kind and $\lambda^2 = \omega^2/c_s^2 - k^2$, with c_s the sound speed, if the ambient medium is assumed to be unmagnetized. The perturbed jet is assumed to remain in equilibrium with its surroundings. Regularity on the axis provides the other boundary condition, *i.e.*, $Y = 0$ for $r = 0$.

REFERENCES

- Appl S., 1996, A&A 314, 995
 Appl S., Camenzind C., 1993, A&A 274, 699
 Appl S., Lery T., Baty H., 1999, A&A, submitted
 Bahcall J.N., Kirhakos S., Schneider D.P., Davis R.J., Muxlow T.W.B., Garrington S.T.,
 Conway R.G., 1995, ApJ, 452, L91
 Bacciotti F., Eisloffel J., 1999, A&A 342, 717

- Begelman M.C., 1998, ApJ 493, 291
- Belcher J.W., MacGregor K.B., 1976, ApJ 210, 498
- Bertout C., Basri G., Bouvier J., 1988, ApJ 330, 350
- Beskin, V.S., Kuznetsova, I.V., Rafikov, R.R., 1998, MNRAS 299, 341
- Biretta, J.A., 1996, in *Energy Transport in Radio Galaxies and Quasars*, Eds. P. Hardee, A. Bridle, J.A. Zensus, NRAO (Greenbank), p. 187
- Blandford R.D., Payne D.G., 1982, MNRAS 199, 883
- Bodo G., Massaglia S., Rossi P., Rosner R., Malagoli A., Ferrari A., 1995, A&A 303, 281
- Bogovalov S., 1995, Astron. Letts, 21, 4
- Bogovalov S., Tsinganos K., 1999, MNRAS, in press
- Burke T., Mundt R., Ray T.P., 1988, A&A 200,99
- Camenzind M., 1990,in *Reviews of Modern Astronomy 3*, ed. G. Klare, Springer-Verlag (Heidelberg), p.234
- Camenzind M., 1997, IAUS 182, 241
- Cerqueira A. H., Gouveia Dal Pino E. M., & Herant M., 1999 ApJ, in press
- Contopoulos J., Lovelace R.V.E., 1994, ApJ 429, 139
- Dutrey A., Langer W.D., Bally J., Duvert G., Castets A., Wilson R.W., 1991, A&A 247, L9
- Eisloffel J., Mundt R., 1997, AJ 114, 280
- Elmegreen B.G., 1989, ApJ, 338,178
- Fendt C., Camenzind M., 1996, A&A 313, 591
- Feretti L., Perley R., Giovannini G., Andernach H., 1999, A&A 341, 29
- Ferreira J., Pelletier G., 1993a, A&A 276, 625
- Ferreira J., 1997, A&A 319, 340
- Fiege J.D., Henriksen R.N., 1996, MNRAS 281, 1038
- Frank A., Mellema G., 1996, ApJ 472, 684

- Frank A., Ryu D., Jones T. W. & Noriega-Crespo A. 1998, ApJ, 494, L79
- Frank A., Lery, T., Gardiner T.A., Ryu D., Jones T. W. ApJ, submitted
- Frank A., Gardiner T.A., Delemarter G., Lery T., Betti R., 1999, ApJ, in press
- Gardiner T., Frank A., Ryu D., Jones T., 1999, ApJ, submitted
- Heyvaerts, J & Norman, C., 1989, ApJ, 347, 1055
- Kennel C.F., Fujimura F.S., Okamoto I., 1983, Geophys. Astrophys. Fluid Dynamics, 26, 147
- Krichbaum T.P., Hummel C.A., Quirrenbach A., et al., 1990, A&A, 230, 271
- Lery T., 1996, Ph.D. Thesis, ULP Strasbourg
- Lery T., Baty H., Appl S., 1999c, A&A submitted
- Lery T., Henriksen R.N., Fiege J.D., 1999b, A&A, in press
- Lery T., Heyvaerts J., Appl S., Norman C.A., 1998, A&A 337, 603
- Lery T., Heyvaerts J., Appl S., Norman C.A., 1999a, A&A, 347, 1055
- Lynden-Bell D., 1996, MNRAS 279, 389
- Micono M., Massaglia S., Bodo G., Rossi P., Ferrari A., 1998, A&A 333, 1001
- Morse J.A., Heathcote S.R., Hartigan P., Cecil G., 1993, AJ 106, 1139
- Ostriker E.C., 1997, ApJ, 486, 291
- Pelletier G., Pudritz R.E., 1992, ApJ 394, 117
- Raga A., Noriega-Crespo A., 1998, AJ 116, 2943
- Ray T.P., Mundt R., Dyson J.E., Falle S.A.E.G., Raga A.C., 1996, ApJ 468, L103
- Reipurth B., 1989, Nature 340, 42
- Reipurth B., Bally J., Devine D., 1997, ApJ 114, 2708.
- Rosado M., Raga A.C., Arias L., 1999, AJ 117, 462
- Ryu D., Jones T.W., Frank A., 1995a, ApJ 452, 785

- Ryu, D., Yun, H. S., Choe, S. 1995b, *J. Korean Ast. Soc.*, 28, 243.
- Sakurai T., 1987, *PASJ* 39, 821
- Sauty C., Tsinganos K., 1994, *A&A* 287, 893
- Schwartz R.D., Greene T.P., 1999, *AJ* 117, 456
- Shu F.H., Lizano S., Ruden S.P., Najita J., 1988, *ApJ* 328, L19
- Shu F.H., Najita J., Ostriker E., Wilkin F., Ruden S. and Lizano S., 1994, *ApJ* 429, 781
- Shu F.H., Najita J., Ostriker E., Shang H., 1995, *ApJ*, 455, L155
- Stone J, & Hardee P., 1999, preprint
- Todo Y., Uchida Y., Sato T., Rosner R., 1992, *PASJ* 44, 245
- Trussoni E., Tsinganos K., Sauty C., 1997, *A&A*, 325,1099
- Vlahakis N., Tsinganos K., 1998, *MNRAS* 298, 777
- Weber E.J., Davis L., 1967, *ApJ* 148, 217

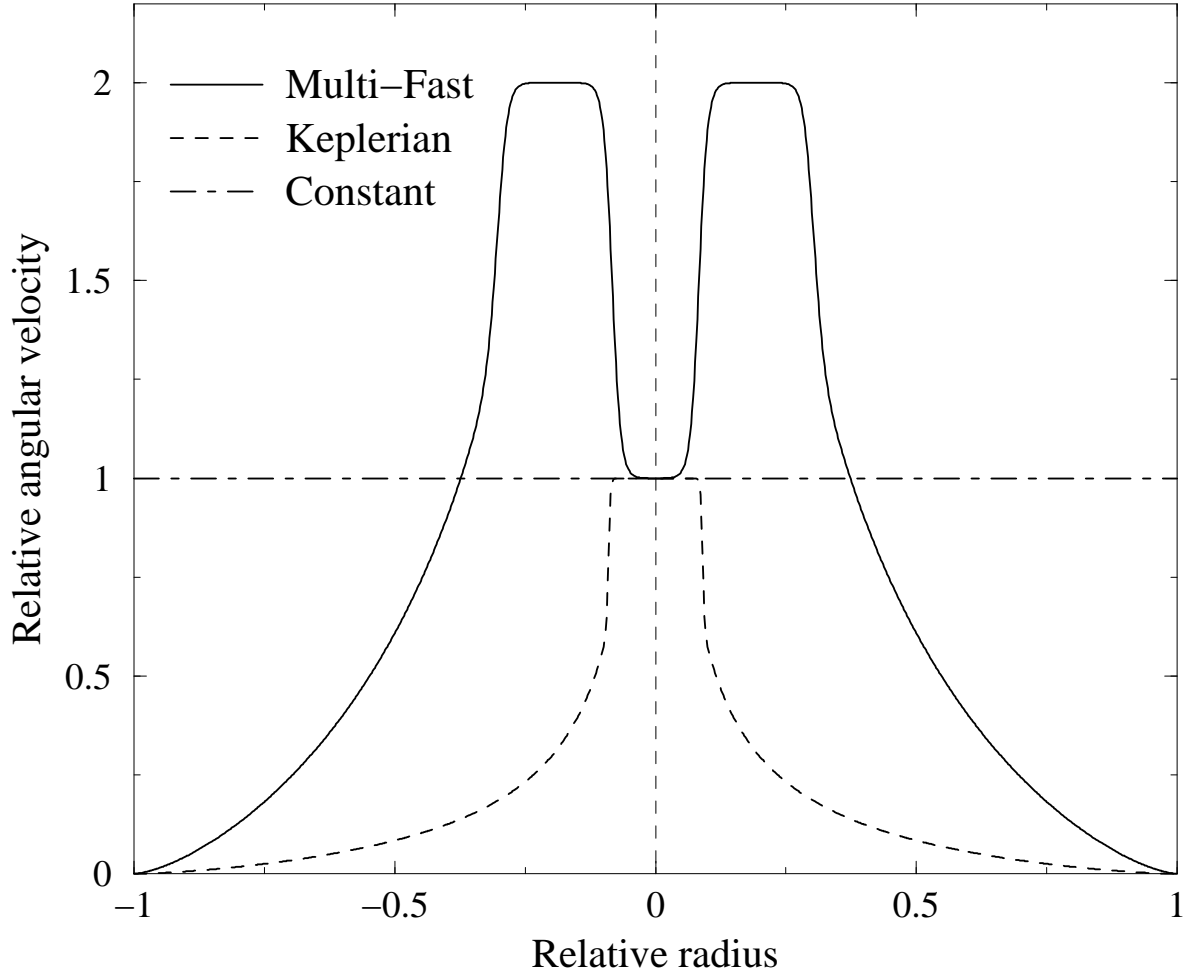


Fig. 1.— Rotation laws for constant (dot-dashed), pure *Keplerian* (dashed), and multi-components, or *multi-fast*, (solid) models. Axial angular velocity is set to unity.

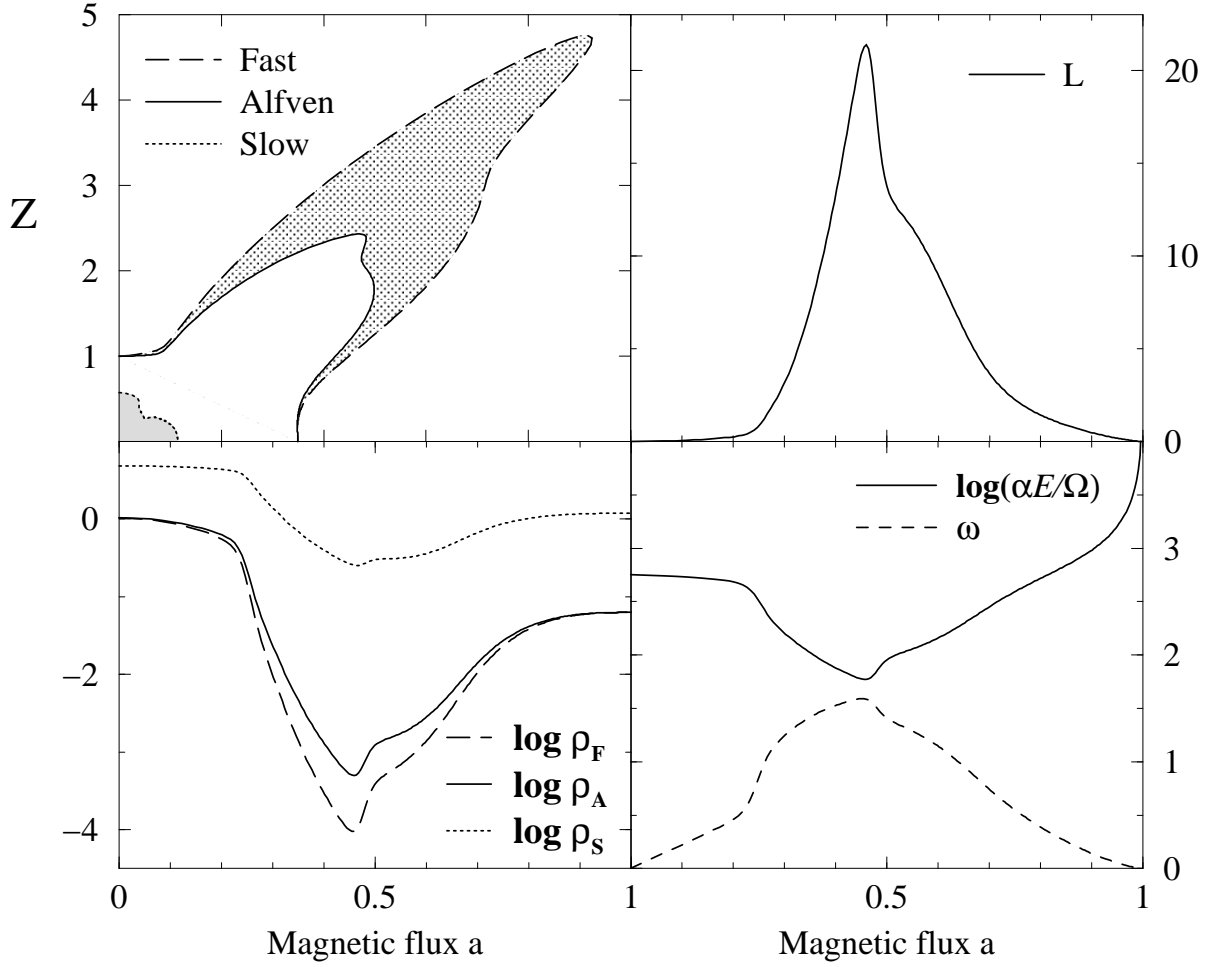


Fig. 2.— *Multi-fast case* : We show the critical surfaces in dimension-less quantities (upper left), and the densities on these surfaces (lower left). Three first integrals, namely the total angular momentum L (upper right), the rotation parameter ω and the ratio $\alpha E/\Omega$ (lower right) are calculated on the Alfvénic surface as functions of the magnetic flux a . Input parameters are $\bar{Q} = 0.87$, $\bar{\Omega} = 2$ and $\bar{\alpha}_0 = 0.7$ ($\gamma \approx 1$).

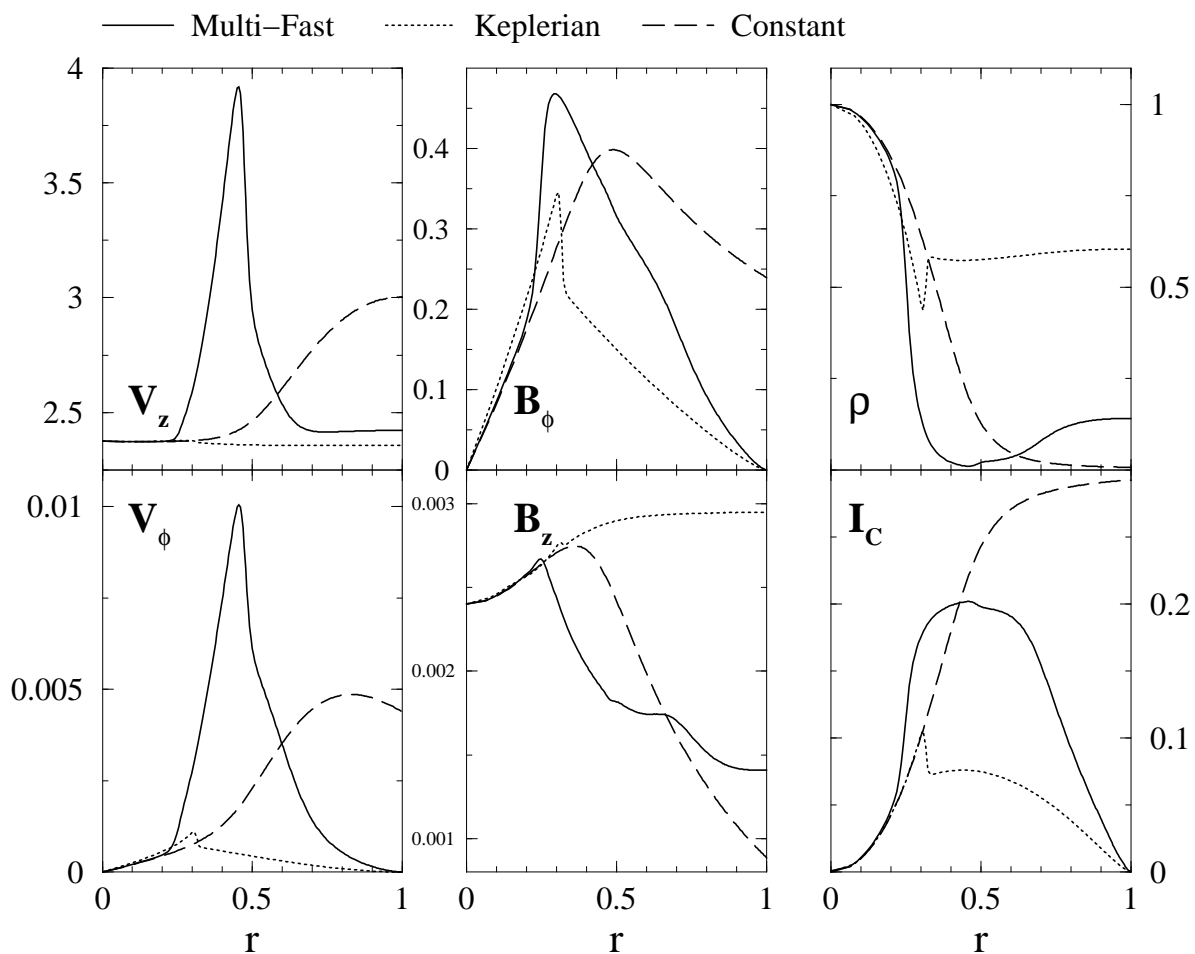


Fig. 3.— Variations with the relative radius of the velocity V and magnetic field B components, of the density ρ and of the net electric current I_C in the *cylindrically collimated regime*. Constant (dotted lines), pure *Keplerian* (dashed), and *multi-fast* (solid) rotation laws are considered.

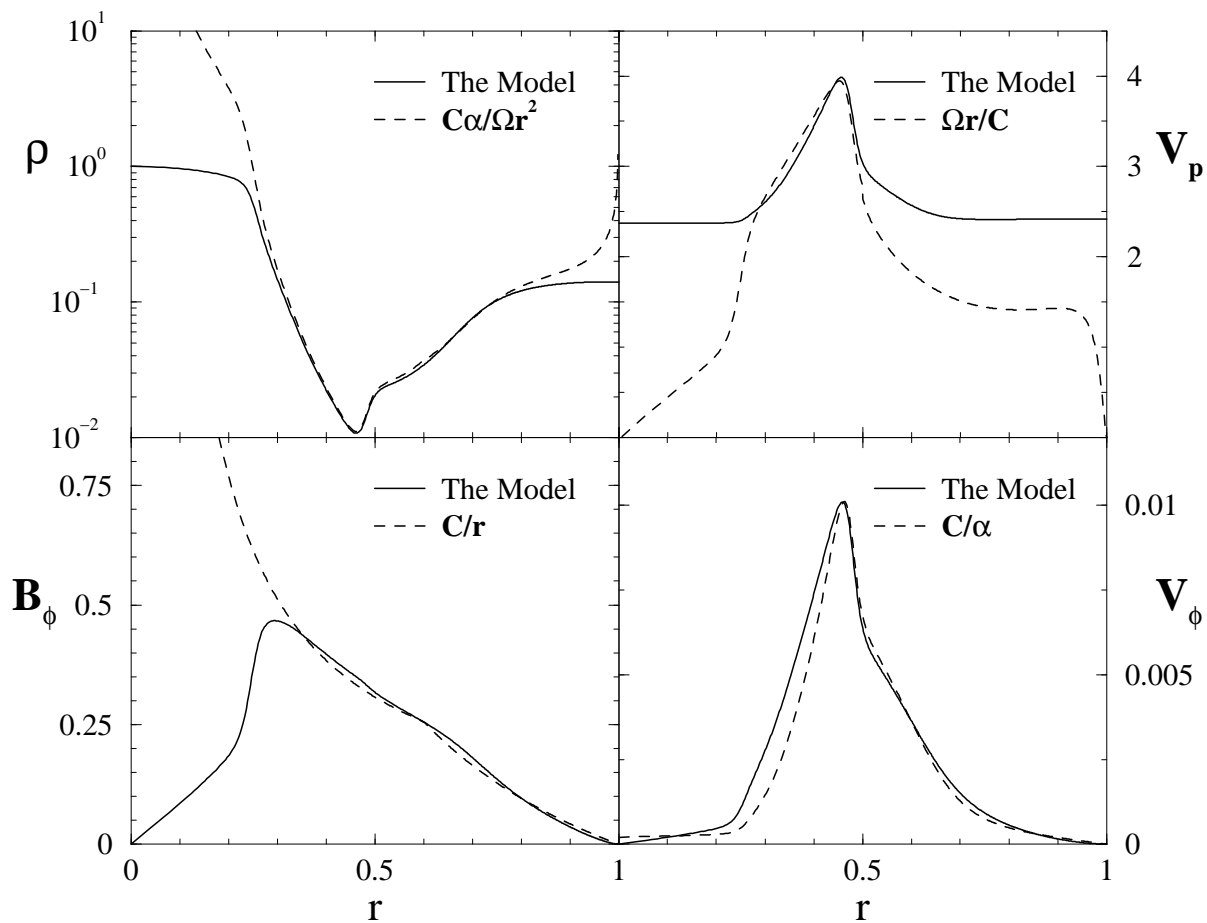


Fig. 4.— Jet variable distributions for *multi-fast* (solid line) and approximate analytical (dashed line) solutions in the asymptotic region as functions of the relative radius.

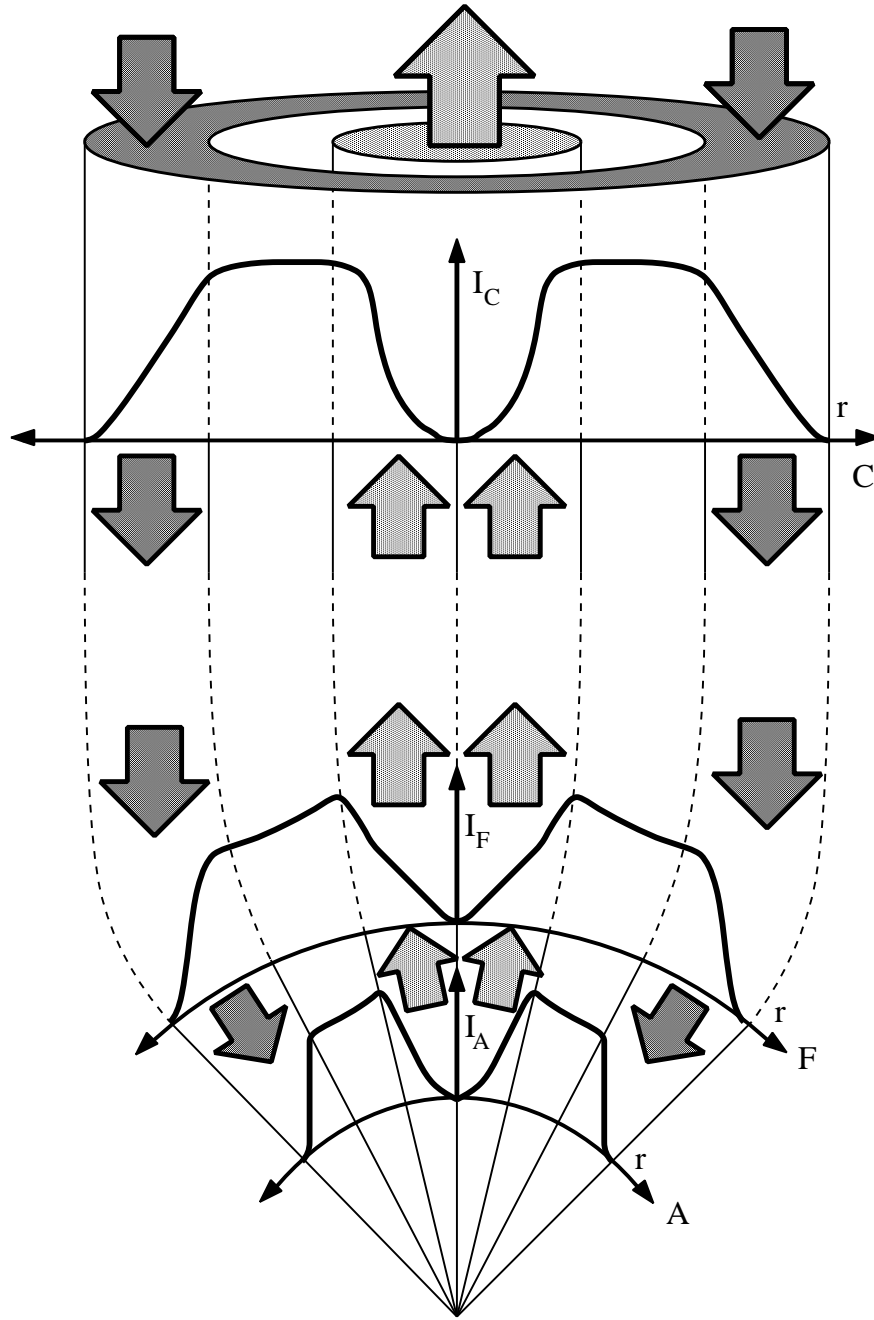


Fig. 5.— Schematic representation of the variations of the net electric current along the jet (heavy solid lines), and its direction (arrows), at the Alfvénic (A), and the fast (F) surfaces, and in the cylindrically collimated regime (C). The light solid (and dashed) lines represent the poloidal projection of magnetic field lines.

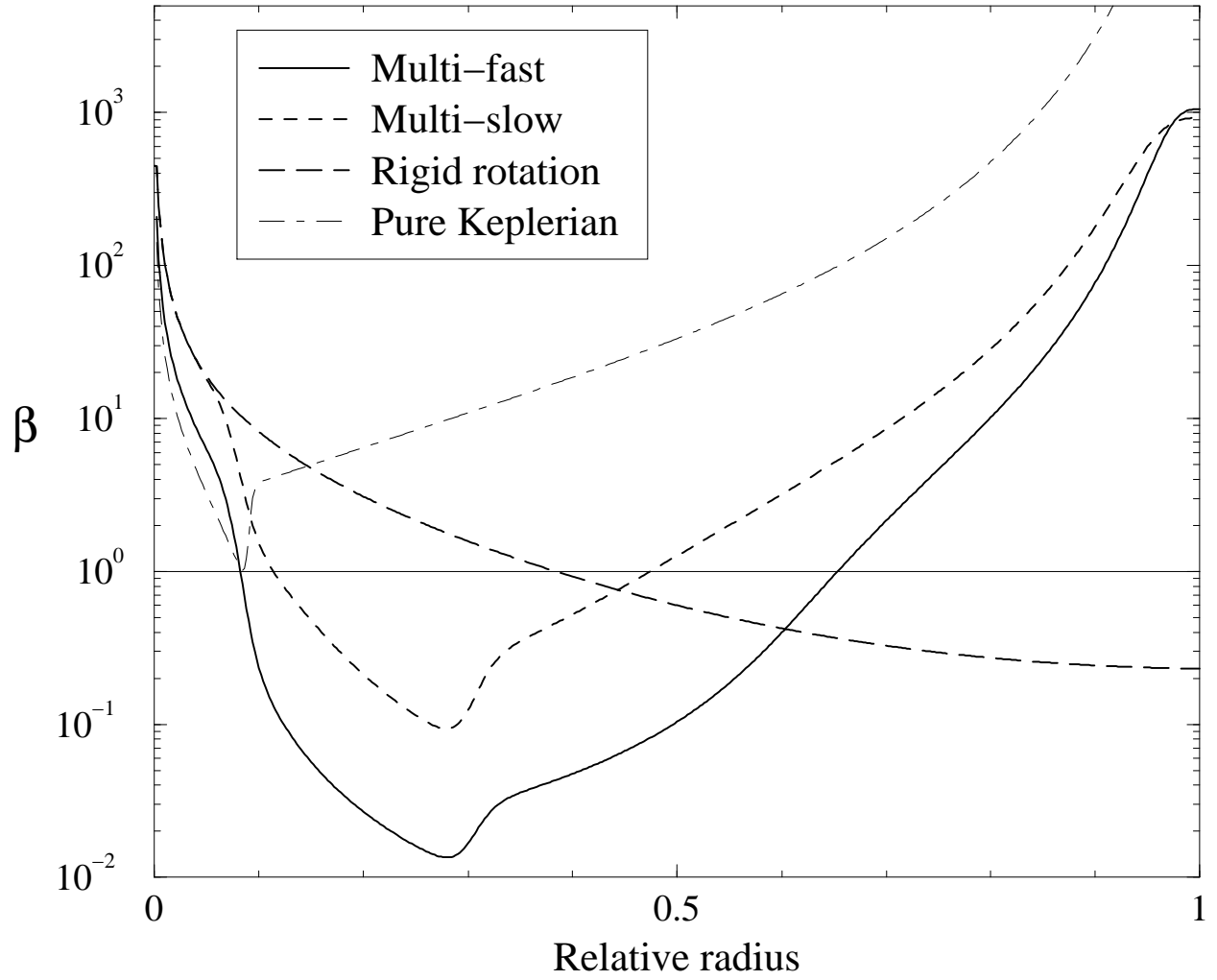


Fig. 6.— Plasma β parameter as a function of the relative radius for the *multi-fast* (solid), *multi-slow* (dashed), rigid body (long dashed) and pure *Keplerian* (dotted-dashed) rotation cases.

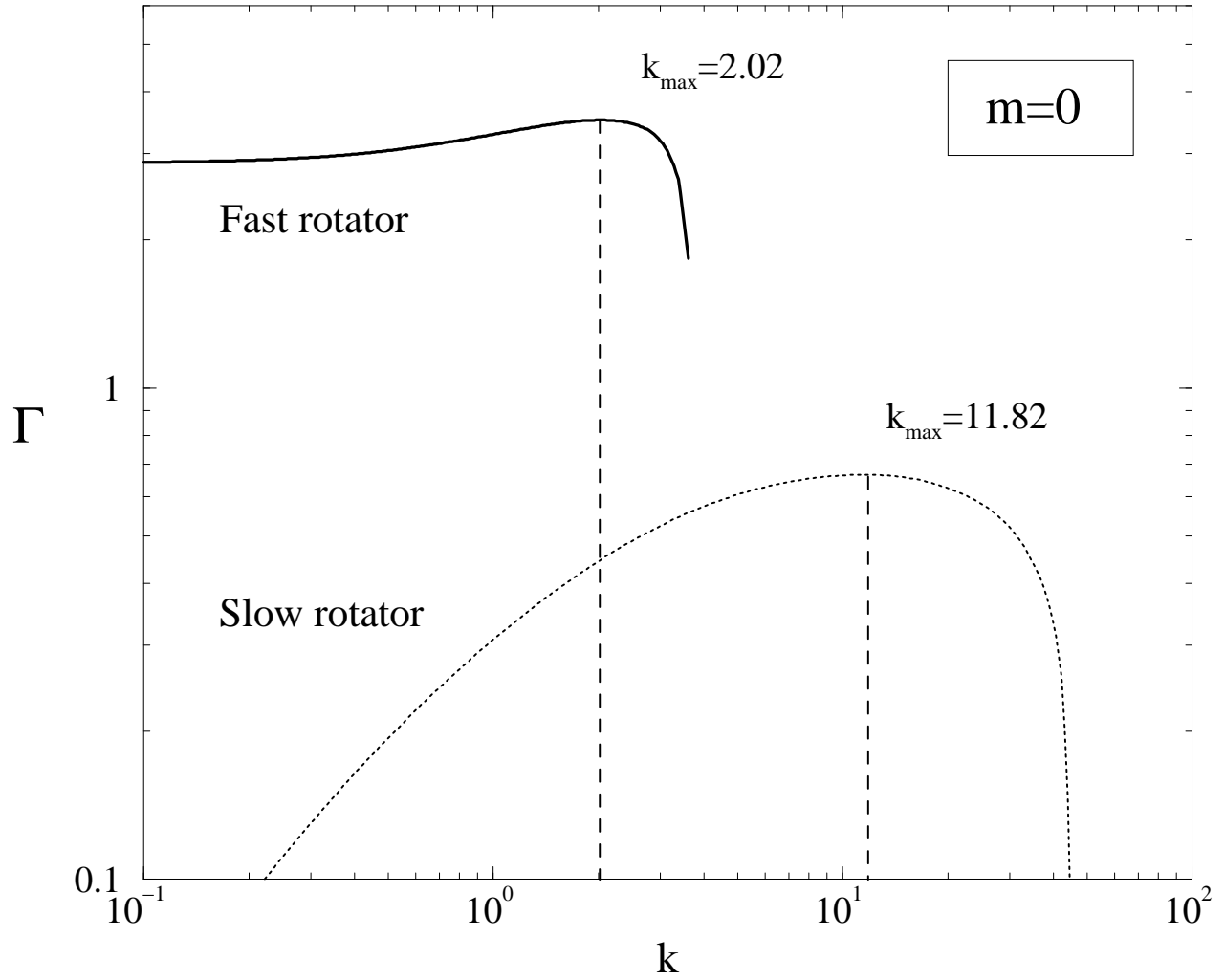


Fig. 7.— Dispersion relation of the pinch mode ($m = 0$) for fast and slow rotators (solid and dotted lines respectively). Dashed lines correspond to the maximum wavenumbers ($k_{max} = 2.02$, $k_{max} = 11.82$).

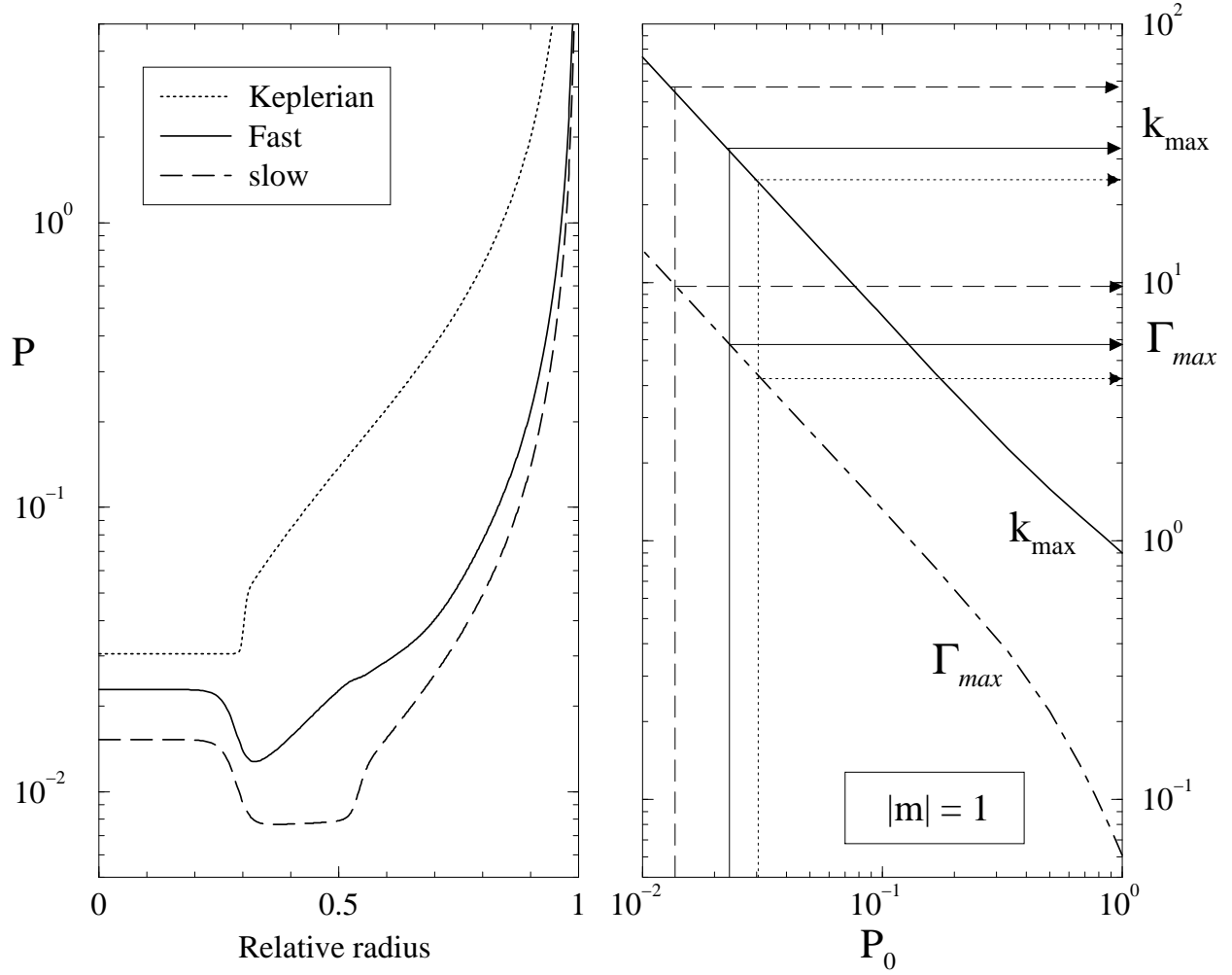


Fig. 8.— The Pitch profile (left panel) is shown for the *Keplerian* (dotted lines), the *multi-fast* (solid), and the *multi-slow* (dashed) cases. On the right panel, the maximum growth rate (Γ_{max}) and the maximum wavenumber (k_{max}) are plotted as functions of the central pitch value. The arrows mark their estimate for the different cases.

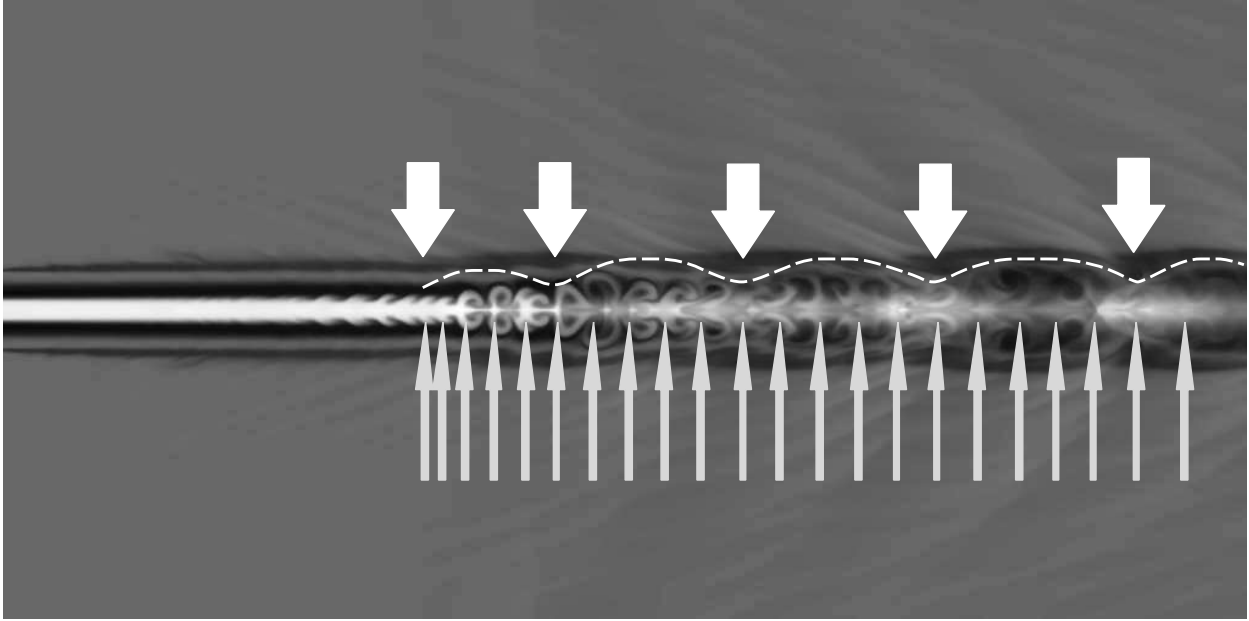


Fig. 9.— Structures of instabilities. Thick white arrows correspond to knots of the envelope (delimited by dashed line), and thin black arrows to maxima of density for the internal instabilities.

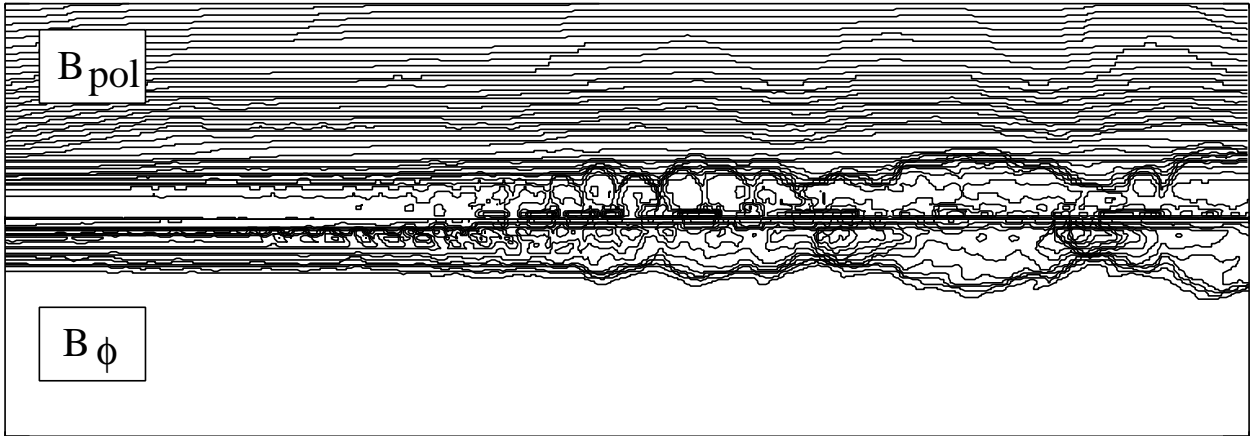


Fig. 10.— Components of the magnetic field of the destabilized equilibrium

Table 1. The Pinch Mode: growth rate Γ_{max} , wave number k_{max} , and wavelength λ_{max} of the instability with the largest growth rate for the slow and the fast rigid body rotators.

type	Γ_{max}	k_{max}	λ_{max}
Fast rotator	3.50	2.02	3.11
Slow rotator	0.67	11.82	0.53

Table 2. The Helical Mode: central pitch P_0 , growth rate Γ_{max} , wavenumber k_{max} , and wavelength λ_{max} of the instability with the largest growth rate for the different rotators.

type	P_0	Γ_{max}	k_{max}	λ_{max}
<i>Keplerian</i>	0.031	4.2	25	0.25
<i>multi-fast</i>	0.023	5.5	30	0.20
<i>multi-slow</i>	0.015	9.5	55	0.11

Table 3. The simulation: number of instabilities N , their size (in units of r_{jet}), their mean wave number $\bar{k} = 2\pi N/size$, and the mean wavelength $\bar{\lambda} = size/N$ for the *multi-fast* case.

type	N	size	\bar{k}	$\bar{\lambda}$
Envelope	3	8.6 ± 0.75	2.19 ± 0.19	2.87 ± 0.25
Core	21	10.5 ± 0.75	12.57 ± 1.00	0.50 ± 0.04

Table 4. Wavelengths of the envelope λ_E , of the core λ_C , and their ratio.

method	λ_E	λ_C	ratio
Stability analysis	3.11	0.53	5.87
Simulation	2.87 ± 0.25	0.50 ± 0.04	5.74 ± 0.96